

Pilot-Assisted Short-Packet Transmission over Multiantenna Fading Channels: A 5G Case Study

Guido Carlo Ferrante¹, Johan Östman¹, Giuseppe Durisi¹, and Kittipong Kittichokechai²

¹Chalmers University of Technology, Gothenburg, Sweden

²Ericsson Research, Ericsson AB, Sweden

Abstract—Leveraging recent results in finite-blocklength information theory, we investigate the problem of designing a control channel in a 5G system. The setup involves the transmission, under stringent latency and reliability constraints, of a short data packet containing a small information payload, over a propagation channel that offers limited frequency diversity and no time diversity. We present an achievability bound, built upon the random-coding union bound with parameter s (Martinez & Guillén i Fàbregas, 2011), which relies on quadrature phase-shift keying modulation, pilot-assisted transmission to estimate the fading channel, and scaled nearest-neighbor decoding at the receiver. Using our achievability bound, we determine how many pilot symbols should be transmitted to optimally trade between channel-estimation errors and rate loss due to pilot overhead. Our analysis also reveals the importance of using multiple antennas at the transmitter and/or the receiver to provide the spatial diversity needed to meet the stringent reliability constraint.

I. INTRODUCTION

Ultra-reliable low-latency communication (URLLC) is one of the new use cases that will be supported in 5G [1]. It involves the transmission of short packets, under latency and reliability constraints that are much more stringent than the ones satisfied by traditional mobile broadband applications. Possible applications include factory automation and traffic safety.

Classical information-theoretic metrics, such as the ergodic and the outage capacity, are not suitable to design URLLC links, because they rely on the assumption of large blocklength, which is typically not compatible with the latency requirements in URLLC links [2]. Instead, the problem of optimally designing such systems can be tackled in a fundamental fashion using the finite-blocklength information-theoretic tools developed by Polyanskiy *et al.* [3].

These tools have recently enabled the characterization of the maximum coding rate achievable, for a given blocklength and a given error probability, over quasi-static fading channels [4], and over multiple-input multiple-output (MIMO) Rayleigh block-fading channels [5]. They have also been used to determine optimum power-control strategies in the presence of channel-state information (CSI) at the transmitter [6], and to bound the rates achievable with pilot-assisted transmission (PAT) followed by scaled nearest-neighbor (SNN) decoding at

the receiver for the single-input single-output (SISO) Rician block-fading channel [7]. In [7], the design of actual channel coding schemes approaching the bounds is also discussed.

Contributions: In this paper, we generalize the analysis in [7] to the case of multiple-antenna transmissions. Specifically, we present an upper bound on the packet error probability attainable at a given blocklength using a channel code of a fixed rate, when communicating over a MIMO block-fading channel.

As in [7], we assume PAT and SNN decoding at the receiver. However, differently from [7], where the analysis relies on the transmission of spherical codes, we focus in this paper on the rates achievable using quadrature phase-shift keying (QPSK) modulation, which is more practically relevant, and also a natural choice given the low levels of spectral efficiency at which 5G URLLC links are expected to operate. We also consider the use of an Alamouti inner code [8] at the transmitter, which constrains the transmit antennas to provide only spatial diversity, which may be crucial to achieve high reliability levels.

Our bound is not in closed form; its evaluation requires Monte Carlo simulations, which may be time consuming if the target error probability is low. To partially overcome this issue, we present an accurate saddlepoint approximation [9], [10] of our bound, which, although not in closed form either, can be computed more efficiently than the bound, because its complexity does not increase with the number of diversity branches available in the channel.

Finally, we use our bound to shed light on the optimal design of a control channel in a 5G system, where the payload is assumed to be 30 bits, the target packet error probability is 10^{-5} and the data packet consists of multiple resource blocks (RBs) in frequency, so as to minimize latency. Furthermore, the spacing between the RBs is chosen so as to optimally exploit the frequency diversity offered by the channel. The coherence time and the coherence bandwidth of the block-fading model are chosen so as to match the ones prescribed by the extended pedestrian type A (EPA) 5 Hz [11] and the tapped delay line type-C (TDL-C) 300 ns–3 km/h [12] channel models. Furthermore, the number and the distribution of the RBs in frequency as well as the number of pilot symbols are optimized. We analyze how the performance of a single-input multiple-output (SIMO) system depends on the number of available receive antennas. We also illustrate that the sensitivity of the Alamouti scheme to imperfect channel estimation makes this scheme unsuitable

This work was partly supported by the Swedish Research Council under grants 2014-6066 and 2016-03293. The simulations were performed in part on resources provided by the Swedish National Infrastructure for Computing (SNIC) at C3SE.

for transmission over channels exhibiting a large amount of frequency selectivity.

Notation: We shall denote vectors and matrices by bold lower and uppercase letters, such as \mathbf{x} and \mathbf{X} , respectively. The identity matrix of size $a \times a$ is written as \mathbf{I}_a . The distribution of a circularly-symmetric complex Gaussian random variable with variance σ^2 is denoted by $\mathcal{CN}(0, \sigma^2)$. The superscripts $(\cdot)^*$, $(\cdot)^T$, and $(\cdot)^H$ denote conjugation, transposition, and Hermitian transposition, respectively. We write $\log(\cdot)$ and $\log_2(\cdot)$ to denote the natural logarithm and the logarithm to the base 2, respectively. Finally, $[a]^+$ stands for $\max\{0, a\}$, $Q(\cdot)$ denotes the Gaussian Q -function, $\|\cdot\|$ the ℓ^2 -norm, $\|\cdot\|_F$ the Frobenius norm, and $\mathbb{E}[\cdot]$ the expectation operator.

II. SYSTEM MODEL

A. Input-Output Relation

We consider a discrete-time MIMO block-fading channel with M_t transmit and M_r receive antennas. Let n_c be the size of each coherence block, i.e., the number of channel uses over which the channel stays constant. We assume that each codeword of length n spans L coherence blocks, i.e., $n = Ln_c$. We shall refer to L as the number of diversity branches. The signal received during block ℓ is

$$\mathbf{Y}_\ell = \mathbf{H}_\ell \mathbf{X}_\ell + \mathbf{W}_\ell, \quad (1)$$

where $\mathbf{Y}_\ell \in \mathbb{C}^{M_r \times n_c}$ is the channel output, $\mathbf{H}_\ell \in \mathbb{C}^{M_r \times M_t}$ is the matrix containing the fading coefficients in the ℓ th coherence block, $\mathbf{X}_\ell \in \mathbb{C}^{M_t \times n_c}$ is the channel input, and $\mathbf{W}_\ell \in \mathbb{C}^{M_r \times n_c}$ is the AWGN matrix. The noise matrices $\{\mathbf{W}_\ell\}$ have independent and identically distributed (i.i.d.) entries drawn from $\mathcal{CN}(0, 1)$ and are independent across ℓ . The fading matrices $\{\mathbf{H}_\ell\}$ are also i.i.d. over ℓ ; their distribution is, however, arbitrary. Furthermore, we assume that $\{\mathbf{H}_\ell\}$ and $\{\mathbf{W}_\ell\}$ are independent, and that they do not depend on $\{\mathbf{X}_\ell\}$. We next define the notion of a channel code.

Definition 1: An (n, M, ϵ) -code consists of:

- An encoder $f : \{1, \dots, M\} \rightarrow \mathbb{C}^{M_t \times n}$ that maps the message J , which is uniformly distributed on the set $\{1, \dots, M\}$ to a codeword $\mathbf{C}_m = f(J) \in \mathbb{C}^{M_t \times n}$ in the codebook set $\{\mathbf{C}_1, \dots, \mathbf{C}_M\}$. Each codeword satisfies the power constraint $\|\mathbf{C}_m\|_F^2 \leq n_c \rho$, $m = 1, \dots, M$.
- A decoder $g : \mathbb{C}^{M_r \times n} \rightarrow \{1, \dots, M\}$ that maps the channel output $\mathbf{Y} = [\mathbf{Y}_1, \dots, \mathbf{Y}_L]$ to a message estimate $\hat{J} = g(\mathbf{Y})$. The decoder satisfies the average packet error probability constraint

$$\Pr\{\hat{J} \neq J\} \leq \epsilon. \quad (2)$$

The maximum coding rate $R^*(n, \epsilon)$ for a given blocklength n and a given error probability ϵ is the largest rate achievable using (n, M, ϵ) -codes:

$$R^*(n, \epsilon) = \sup \left\{ \frac{\log_2 M}{n} : \exists (n, M, \epsilon)\text{-code} \right\}. \quad (3)$$

Similarly, we define the minimum error probability $\epsilon^*(n, R)$ achievable using codes of blocklength n and rate $R = n^{-1} \log_2(M)$ as

$$\epsilon^*(n, R) = \inf \{ \epsilon : \exists (n, \lceil 2^{nR} \rceil, \epsilon)\text{-code} \}. \quad (4)$$

This quantity is often studied as a function of the energy per bit normalized by the noise spectral density, $E_b/N_0 = \rho/R$.

B. PAT and SNN Decoding

We assume that each input matrix \mathbf{X}_ℓ is of the form $\mathbf{X}_\ell = [\mathbf{X}_\ell^{(p)} \mathbf{X}_\ell^{(d)}]$ where $\mathbf{X}_\ell^{(p)} \in \mathbb{C}^{M_t \times n_p}$. Here, $\mathbf{X}_\ell^{(p)}$, with $M_t \leq n_p < n_c$, is a deterministic matrix containing orthogonal pilot sequences in each row. Specifically, we assume that $\mathbf{X}_\ell^{(p)} (\mathbf{X}_\ell^{(p)})^H = (\rho n_p / M_t) \mathbf{I}_{M_t}$. The matrix $\mathbf{X}_\ell^{(d)} \in \mathbb{C}^{M_t \times n_d}$, where $n_d = n_c - n_p$, contains the data symbols.

Let $\mathbf{Y}_\ell^{(p)}$ and $\mathbf{Y}_\ell^{(d)}$ be the matrices containing the received samples that correspond to the pilot and the data symbols within the ℓ th coherence block, respectively. Given $\mathbf{Y}_\ell^{(p)}$ and $\mathbf{Y}_\ell^{(d)}$, the receiver computes the maximum likelihood (ML) estimate $\widehat{\mathbf{H}}_\ell$ of the fading matrix \mathbf{H}_ℓ as

$$\widehat{\mathbf{H}}_\ell = \frac{M_t}{\rho n_p} \mathbf{Y}_\ell^{(p)} (\mathbf{X}_\ell^{(p)})^H. \quad (5)$$

Then, the decoder produces as output the message

$$\hat{J} = \arg \max_{1 \leq m \leq M} q^{(L)}(\mathbf{C}_m, \mathbf{Y}) \quad (6)$$

where

$$q^{(L)}(\mathbf{X}, \mathbf{Y}) = \prod_{\ell=1}^L q(\mathbf{X}_\ell, \mathbf{Y}_\ell) \quad (7)$$

with $\mathbf{X} = [\mathbf{X}_1, \dots, \mathbf{X}_L]$ and

$$q(\mathbf{X}_\ell, \mathbf{Y}_\ell) = \prod_{k=1}^{n_d} \exp(-\|\mathbf{y}_{\ell,k}^{(d)} - \widehat{\mathbf{H}}_\ell \mathbf{x}_{\ell,k}^{(d)}\|^2) \quad (8)$$

is the SNN decoding metric. Here, $\mathbf{y}_{\ell,k}^{(d)}$ and $\mathbf{x}_{\ell,k}^{(d)}$ denote the k th column of the matrices $\mathbf{Y}_\ell^{(d)}$ and $\mathbf{X}_\ell^{(d)}$, respectively.

Some remarks on (8) are in order. When $\widehat{\mathbf{H}}_\ell = \mathbf{H}_\ell$, i.e., when perfect CSI is available at the receiver, the SNN decoding metric $q(\mathbf{X}_\ell, \mathbf{Y}_\ell)$ in (8) is equivalent to the ML metric, which is optimal in the sense that it minimizes the error probability $\Pr\{\hat{J} \neq J\}$. However, using this rule for the case of inaccurate CSI considered in this paper yields a mismatch.

The transceiver architecture just described, which relies on PAT, on ML channel estimation, and on SNN decoding, and which we shall refer to as PAT-ML-SNN coding scheme, is ubiquitous in current wireless systems, although suboptimal. Treating the channel estimate as perfect enables the use of the ‘‘coherent’’ decoding rule (6)–(8), whose performance can be approached in practice using good channel codes for the AWGN channel.

III. BOUNDS ON THE ERROR PROBABILITY

The performance of the PAT-ML-SNN coding scheme just introduced can be analyzed using the mismatch-decoding framework [13]. Specifically, our analysis is based on the RCUs achievability bound [14, Thm. 1], a relaxation of the RCU bound [3, Thm. 16] that recovers the generalized random-coding error exponent for mismatch detection introduced in [15]. Our main result is given in the following theorem.

Theorem 1: Fix an integer $1 \leq n_d < n_c$, a real number $s \geq 0$, and a probability distribution $P_{\mathbf{X}^{(d)}}$ on $\mathbb{C}^{M_t \times n_d}$ for which $\|\mathbf{X}^{(d)}\|_F^2 \leq \rho n_d$ w.p.1 when $\mathbf{X}^{(d)} \sim P_{\mathbf{X}^{(d)}}$. Let the generalized information density $\iota_s(\mathbf{X}_\ell, \mathbf{Y}_\ell)$ be defined as

$$\iota_s(\mathbf{X}_\ell, \mathbf{Y}_\ell) = \log \frac{q(\mathbf{X}_\ell, \mathbf{Y}_\ell)^s}{\mathbb{E}_{\bar{\mathbf{X}}_\ell} [q(\bar{\mathbf{X}}_\ell, \mathbf{Y}_\ell)^s]} \quad (9)$$

where $\bar{\mathbf{X}}_\ell = [\bar{\mathbf{X}}_\ell^{(p)}, \bar{\mathbf{X}}_\ell^{(d)}]$ with $\bar{\mathbf{X}}_\ell^{(p)}$ an arbitrary pilot matrix satisfying the properties listed in Section II-B, and $\bar{\mathbf{X}}_\ell^{(d)} \sim P_{\mathbf{X}^{(d)}}$. The average error probability $\epsilon(n, R)$ achievable with the PAT-ML-SNN coding scheme described in Section II-B is upper-bounded by

$$\begin{aligned} \epsilon(n, R) &\leq \epsilon_{\text{RCUs}}(n, R) \\ &= \mathbb{E} \left[\exp \left(- \left[\left(\sum_{\ell=1}^L \iota_s(\mathbf{X}_\ell, \mathbf{Y}_\ell) \right) - \log(2^{nR} - 1) \right]^+ \right) \right] \end{aligned} \quad (10)$$

where \mathbf{X}_ℓ is distributed as $\bar{\mathbf{X}}_\ell$ and \mathbf{Y}_ℓ is the induced channel output according to (1).

Proof: We consider all codebooks whose codewords have data symbols that are generated independently according to the product distribution built upon $P_{\mathbf{X}^{(d)}}$, and have the pilot symbols $\mathbf{X}_\ell^{(p)}$ in each coherence interval. It follows from [14, Thm. 1] that the error probability, averaged over all codebooks, achievable with the decoding rule (6) is upper-bounded by $\epsilon_{\text{RCUs}}(n, R)$ given in (10). ■

A. Saddlepoint Approximation

When $P_{\mathbf{X}^{(d)}}$ is taken as product distribution, i.e., $P_{\mathbf{X}^{(d)}}(\mathbf{X}^{(d)}) = \prod_{k=1}^{n_d} P_{\mathbf{x}_k^{(d)}}$, where $\mathbf{x}_k^{(d)}$ stands for the k th column of $\mathbf{X}^{(d)}$ —a choice we will focus on in the numerical results reported in Section IV—the generalized information density takes the following form:

$$\begin{aligned} \iota_s(\mathbf{X}_\ell, \mathbf{Y}_\ell) &= \sum_{k=1}^{n_d} \left\{ -s \|\mathbf{y}_{\ell,k}^{(d)} - \widehat{\mathbf{H}}_\ell \mathbf{x}_{\ell,k}^{(d)}\|^2 \right. \\ &\quad \left. - \log \mathbb{E} \left[\exp \left(-s \|\mathbf{y}_{\ell,k}^{(d)} - \widehat{\mathbf{H}}_\ell \mathbf{x}_{\ell,k}^{(d)}\|^2 \right) \right] \right\}. \end{aligned} \quad (11)$$

Even in this case, though, $\epsilon_{\text{RCUs}}(n, R)$, does not admit in general a closed-form expression. This makes its computation challenging for low error probabilities. To partly overcome this issue, we present next a saddlepoint approximation of $\epsilon_{\text{RCUs}}(n, R)$, which we will show in Section IV to be remarkably accurate over a large range of channel and system parameters. We obtain this approximation by proceeding as in [14, Sec. IV.B] (see also [10,

Sec. V], where the error in the approximation is analyzed). The resulting saddlepoint approximation of $\epsilon_{\text{RCUs}}(n, R)$ is

$$\begin{aligned} \epsilon_{\text{RCUs}}(n, R) &\approx \exp \left(-L [E_0(\hat{\tau}, s) - \hat{\tau} E'_0(\hat{\tau}, s)] \right) \\ &\quad \cdot \left\{ Q \left(\hat{\tau} \sqrt{-L E''_0(\hat{\tau}, s)} \right) e^{-\frac{L}{2} E''_0(\hat{\tau}, s) \hat{\tau}^2} \right. \\ &\quad \left. + Q \left((1 - \hat{\tau}) \sqrt{-L E''_0(\hat{\tau}, s)} \right) e^{-\frac{L}{2} E''_0(\hat{\tau}, s) (1 - \hat{\tau})^2} \right\} \end{aligned} \quad (12)$$

where the Gallager's generalized E_0 function is

$$E_0(\tau, s) = -\log \mathbb{E} \left[e^{-\tau \iota_s(\mathbf{X}_1, \mathbf{Y}_1)} \right], \quad (13)$$

and E'_0 and E''_0 denote the first and the second partial derivatives of E_0 with respect to τ , respectively. The parameter $\hat{\tau}$ in (12) is

$$\hat{\tau} = \arg \max_{\tau \in (0, 1)} \left\{ E_0(\tau, s) - \tau \frac{\log(2^{nR} - 1)}{L} \right\}. \quad (14)$$

A closed form expression for (13) and its partial derivatives is in general not available. Hence, we shall turn to Monte Carlo methods to evaluate (12). Note, that, due to the block-memoryless assumption, the numerical complexity of the approximation in (12) is independent of the number of diversity branches L . In contrast, the complexity of the numerical evaluation of $\epsilon_{\text{RCUs}}(n, R)$ in (10) increases with L .

B. The SIMO Case

In the SIMO case, the SNN decoding metric (8) reduces to

$$q(\mathbf{x}_\ell, \mathbf{Y}_\ell) = \prod_{k=1}^{n_d} \exp \left(-\|\mathbf{y}_{\ell,k}^{(d)} - \widehat{\mathbf{h}}_\ell x_{\ell,k}^{(d)}\|^2 \right). \quad (15)$$

To simplify the computation of (10), it is convenient to left-multiply the vector $\mathbf{y}_{\ell,k}^{(d)} - \widehat{\mathbf{h}}_\ell x_{\ell,k}^{(d)}$ by a unitary matrix whose first row is $\widehat{\mathbf{h}}_\ell^H / \|\widehat{\mathbf{h}}_\ell\|$. This corresponds to performing maximum-ratio combining at the receiver, based on the estimated CSI $\widehat{\mathbf{h}}_\ell$. Since all the entries of the rotated vectors but the first one do not depend on $x_{\ell,k}$ they can be dropped when solving (6). This is equivalent to applying the RCUs bound in Theorem 1 to the following setup: i) the channel (1) is replaced by the block-fading SISO channel

$$\mathbf{y}_\ell^T = \frac{\widehat{\mathbf{h}}_\ell^H \mathbf{h}_\ell}{\|\widehat{\mathbf{h}}_\ell\|} \mathbf{x}_\ell^T + \mathbf{w}_\ell^T \quad (16)$$

where the vectors \mathbf{y}_ℓ , \mathbf{x}_ℓ , and \mathbf{w}_ℓ have n_d entries; furthermore, the vector \mathbf{h}_ℓ contains the M_r channel coefficients in the ℓ th coherence block and $\widehat{\mathbf{h}}_\ell$ is its ML estimate. ii) The decoding metric $q(\cdot, \cdot)$ in (8) is replaced by

$$q(\mathbf{x}_\ell, \mathbf{y}_\ell) = \prod_{k=1}^{n_d} \exp \left(-|y_{\ell,k} - \|\widehat{\mathbf{h}}_\ell\| x_{\ell,k}|^2 \right). \quad (17)$$

C. Spatial Diversity through Alamouti

We next focus on the 2×2 MIMO setup, and discuss the scenario in which an Alamouti inner code is used to obtain spatial diversity from the two available transmit antennas. Let $\mathbf{x}_\ell \in \mathbb{C}^{n_d}$, with $\|\mathbf{x}_\ell\|^2 \leq n_d \rho / 2$, be the vector of data symbols to be transmitted over the coherence block ℓ . Through this section, we shall assume that n_d is even. The data matrix $\mathbf{X}_\ell^{(d)} \in \mathbb{C}^{2 \times n_d}$ is constructed as

$$\mathbf{X}_\ell^{(d)} = \begin{bmatrix} \mathbf{x}_\ell^T \\ e(\mathbf{x}_\ell)^T \end{bmatrix}. \quad (18)$$

Here, the function $e : \mathbb{C}^{n_d} \rightarrow \mathbb{C}^{n_d}$ maps an input vector \mathbf{a} into an output vector \mathbf{b} according to the Alamouti rule [8]

$$[\mathbf{b}]_{2k-1} = [e(\mathbf{a})]_{2k-1} = [\mathbf{a}]_{2k}^* \quad (19)$$

$$[\mathbf{b}]_{2k} = [e(\mathbf{a})]_{2k} = -[\mathbf{a}]_{2k-1}^* \quad (20)$$

for $k = 1, \dots, n_d/2$. Exploiting the structure of the data matrix, one can show that, for the case of perfect CSIR, the performance of this scheme is equal to that of a 1×4 SIMO system where the power of the data symbols is halved.

This is, however, no longer the case when the CSI is acquired through pilot symbols, and hence, inaccurate. In this case, the performance of this coding scheme can be analyzed by applying the RCUs bound in Theorem 1 to an equivalent channel and decoding metric we shall specify next. Let $\tilde{\mathbf{x}}_{\ell,k}$ be a 2-dimensional vector obtained from \mathbf{x}_ℓ by taking the symbol in position $2k - 1$ and the complex conjugate of the symbols in position $2k$, $k = 1, \dots, n_d/2$. We apply the RCUs bound to the equivalent channel

$$\mathbf{y}_{\ell,k} = \frac{1}{\|\widehat{\mathbf{H}}_\ell\|_F} \left(\widehat{\mathbf{V}}_{\ell,1}^H \mathbf{V}_{\ell,1} + \widehat{\mathbf{V}}_{\ell,2}^H \mathbf{V}_{\ell,2} \right) \tilde{\mathbf{x}}_{\ell,k} + \mathbf{w}_{\ell,k} \quad (21)$$

where

$$\mathbf{V}_{\ell,j} = \begin{bmatrix} h_{\ell,1,j} & h_{\ell,2,j} \\ h_{\ell,2,j}^* & -h_{\ell,1,j}^* \end{bmatrix} \quad (22)$$

with $h_{\ell,i,j} = [\mathbf{H}_\ell]_{i,j}$, $i \in \{1, 2\}$, $j \in \{1, 2\}$. The matrix $\widehat{\mathbf{V}}_{\ell,j}$ is defined as in (22), with the entries of \mathbf{H}_ℓ replaced by the entries of its ML estimate $\widehat{\mathbf{H}}_\ell$.

Furthermore, we use the symbol-wise mismatch decoding metric

$$q(\tilde{\mathbf{x}}_\ell, \mathbf{y}_\ell) = \prod_{k=1}^{n_d} \exp(-|y_{\ell,k} - \|\widehat{\mathbf{H}}_\ell\|_F \tilde{x}_{\ell,k}|^2). \quad (23)$$

IV. NUMERICAL RESULTS

We consider a target packet error probability of $\epsilon = 10^{-5}$, in line with the specifications for URLLC [16], a payload of $k = 30$ bits, which models the so-called *compact downlink control information* (DCI) [17], and a blocklength $n = 288$ symbols. This results in a rate of $R = k/n = 0.104$ bit/channel use. Our goal is to identify the system parameters (number of antennas, number of pilot symbols, and distributions of the symbols in the time-frequency plane) that allow us to meet the above requirements. To do so, we use the RCUs bound in Theorem 1.¹

¹Throughout this section, we set $s = 1$ in (10) for simplicity. An optimization over $s \geq 0$ is left for future works.

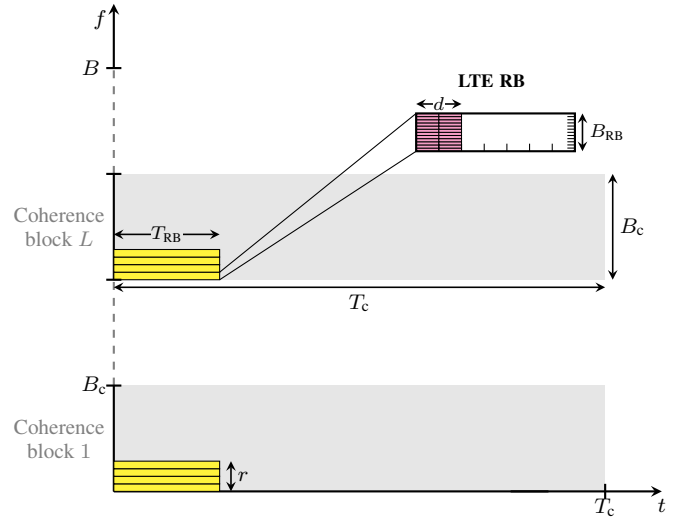


Fig. 1. Channel and signal properties in the time-frequency plane.

TABLE I
CHANNEL (UPPER HALF) AND SIGNAL (BOTTOM HALF) PARAMETERS.

Symbol	Parameter	EPA 5 Hz	TDL-C 300 ns–3 km/h
B_c	50% coh. bandwidth	4.4 MHz	0.66 MHz
T_c	50% coh. time	85 ms	85 ms
L_{\max}	Max no. div. branches	4	30
L	No. div. branches	4	12
n_c	Coh. block size	72	24
n	Blocklength	288	288

For the sake of concreteness, we take as input distribution independent QPSK signaling and assume that the pilot and the data symbols are transmitted at the same power level. Also we focus on $1 \times M_r$ SIMO, with $M_r \in \{1, 2, 4\}$ and on 2×2 MIMO with Alamouti.

We assume the use of orthogonal frequency-division multiplexing (OFDM) with an LTE numerology. This means that each codeword is assigned a number of RBs, each one consisting of d OFDM symbols spanning 12 subcarriers. For a typical downlink control channel transmission in LTE, d is between 1 and 3. As shown in Fig. 1, we allow the RBs to be separated in frequency, but not in time, to benefit from frequency diversity and to limit the transmission delay.

We consider two channel models, which yield a different number of available diversity branches: the EPA 5 Hz [11] and the TDL-C 300 ns–3 km/h [12]. To map these channel models into the block-memoryless fading model (1), we compute their coherence bandwidth B_c and their coherence time T_c . These values are given in Table I. Note that the system bandwidth in LTE is $B = 20$ MHz and that an RB lasts 0.5 ms and occupies $B_{RB} = 180$ kHz. This means that the two channels offer no time diversity and a maximum number of diversity branches $L_{\max} = \lfloor B/B_c \rfloor$, which is 4 for the EPA 5 Hz and 30 for the TDL-C 300 ns–3 km/h. Throughout this section, we focus on Rayleigh fading, i.e., \mathbf{H}_ℓ in (1) has i.i.d. $\mathcal{CN}(0, 1)$ entries. Since

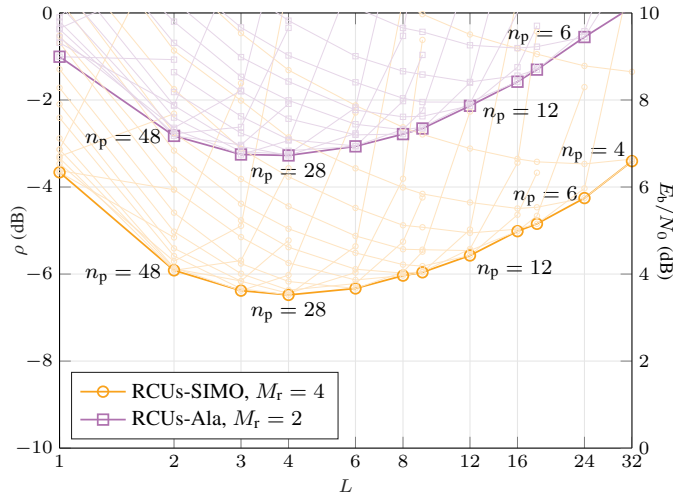


Fig. 2. Minimum SNR to achieve $\epsilon = 10^{-3}$ as a function of the number of frequency diversity branches used: each curve corresponds to a different number of pilot symbols. The optimal number of pilots is reported near some of the points of the envelope.

the noise variance is also 1, we can interpret ρ as the SNR at each receive antenna.

In order to obtain an equivalent block-fading model, we limit the number of RBs per coherence bandwidth to $r \leq B_c/B_{RB}$. The size of the coherence interval n_c in (1) is thus $n_c = 12dr$. Choosing $L = 4$ for the EPA 5 Hz results for example in $n_c = 72$, which can be obtained by setting $d = 2$ and $r = 3$. Similarly, choosing $L = 12$ for the TDL-C 300 ns–3 km/h results in $n_c = 24$, which corresponds to $d = 2$ and $r = 1$.

To illustrate how performance is affected by the choice of the number of diversity branches, we depict in Fig. 2 the minimum SNR needed to achieve 10^{-3} as a function of available diversity branches for the SIMO 1×4 and the Alamouti 2×2 . Each shaded curve in the plot corresponds to a different number of pilot symbols, and the envelope corresponds to the optimal number of pilots. We observe that $L = 4$ yields the lowest SNR value for both systems. However, the curves are rather flat around their minimum. For example, ρ lies within 0.5 dB from its minimum value for all L between 2 and 9.

We next focus on the EPA 5 Hz channel and plot in Figs. 3 and 4 the packet error probability as a function of the number of pilot symbols and the SNR, respectively. Motivated by our findings in Fig. 2, we consider the case $L = 4$, which is the maximum amount of frequency diversity offered by this channel (see Table I). In Fig. 3, we report the error probability as a function of the number of pilot symbols for SIMO and Alamouti. Here, $\rho = -4$ dB. We observe that the error probability is extremely sensitive to changes in the number of pilot symbols. For example, in the SIMO 1×4 case, reducing the number of pilot symbols from its optimal value of 28 to 22, which corresponds to a reduction in the fraction $f_p = n_p/n_c$ of pilot symbols of 8.3%, doubles the error probability.

In Fig. 4, we plot the error probability for the optimal fraction of pilot symbols found in Fig. 3. Each curve is computed for

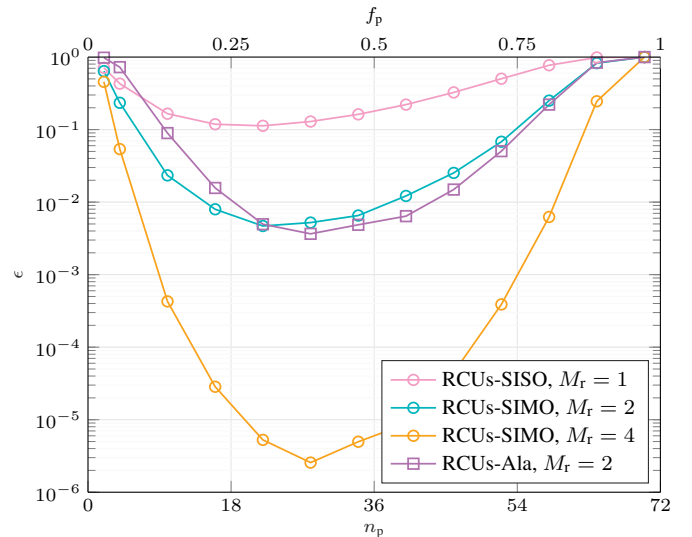


Fig. 3. Error probability vs. number of pilots (bottom axis) or fraction of pilots (top axis) for $\rho = -4$ dB (equivalent to $E_b/N_0 = 6$ dB) for the EPA 5 Hz block-equivalent model.

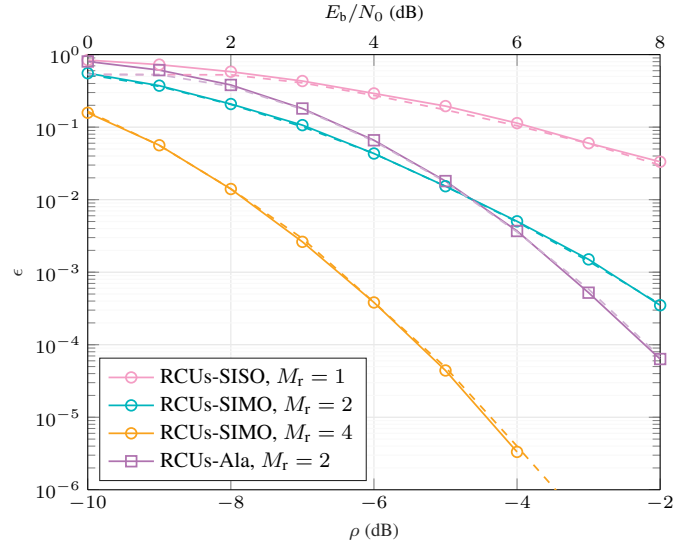


Fig. 4. Error probability vs. SNR (bottom axis) or E_b/N_0 (top axis) for the EPA 5 Hz block-equivalent model. Solid lines: RCUs bound (10); dashed lines: saddlepoint approximation (12).

the optimal fraction of pilots of the corresponding scheme. We also depict the corresponding saddlepoint approximations (12), which turn out to be extremely accurate. As expected, the SIMO 1×4 and the Alamouti 2×2 curves have the same slope because these two setups provide the same amount of space-frequency diversity. The gap is around 3 dB—the expected gap for the case of perfect CSIR. This implies that the channel estimate is sufficiently accurate. We conclude from Figs. 3 and 4 that the only system able to meet the target packet error probability of 10^{-5} within the range of SNR values considered in the figures is the SIMO 1×4 .

We now move to the TDL-C 300 ns–3 km/h, which offers a

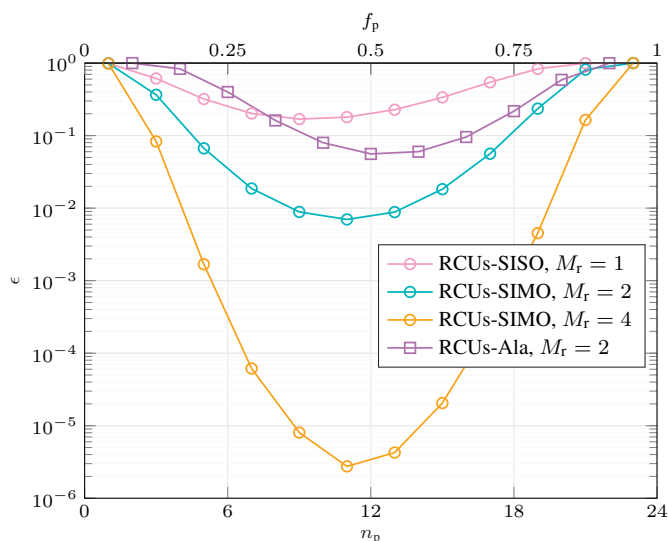


Fig. 5. Error probability vs. number of pilots (bottom axis) or fraction of pilots (top axis) for $\rho = -4$ dB (equivalent to $E_b/N_0 = 6$ dB for the TDL-C 300 ns–3 km/h block-equivalent model).

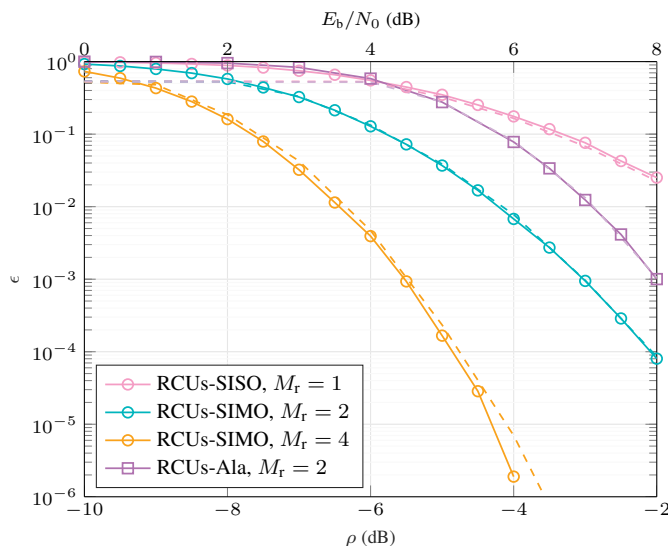


Fig. 6. Error probability vs. SNR (bottom axis) or E_b/N_0 (top axis) for the TDL-C 300 ns–3 km/h block-equivalent model. Solid lines: RCUs bound (10); dashed lines: saddlepoint approximation (12).

larger maximum number of diversity branches in frequency. We assume that the system is designed so that $L = 12$ (see Table I for a complete list of system parameters). Although the analysis reported in Fig. 2 points out that $L = 4$ should be chosen to minimize the SNR (at least at a target packet error probability of 10^{-3}), investigating the case $L = 12$ allow us to assess the impact of frequency selectivity on the performance of the SIMO and the Alamouti schemes.

Figs. 5 and 6 parallel Figs. 3 and 4, respectively, with $L = 12$ instead of $L = 4$. Comparing Figs. 3 and 5, we see that, although the optimal number of pilot symbol is smaller when $L = 12$, because the coherence block is smaller, the fraction of

pilot symbols f_p is actually larger. We also observe that when the number of pilot symbols is chosen optimally, the minimum error probability achievable in the SIMO case when $L = 12$ is similar to when $L = 4$. On the contrary, the error probability of the Alamouti 2×2 scheme increases by an order of magnitude when moving from $L = 4$ to $L = 12$. This is because the Alamouti scheme is more sensitive to imperfect channel estimation, due to the processing needed to extract diversity from the two transmit antennas, i.e., the left-multiplication by the matrices $\hat{\mathbf{V}}_{\ell,1}^H$ and $\hat{\mathbf{V}}_{\ell,2}^H$ in (21). This effect is also illustrated in Fig. 6, where we see that the gap between Alamouti and SIMO 1×4 is now 3.5 dB, instead of the 3 dB loss we observed in Fig. 4. Indeed, for this scenario better performance can be achieved within the range of SNR values depicted in the figure using a SIMO 1×2 , i.e., switching off one of the two transmit antennas.

REFERENCES

- [1] ITU-R, “Report ITU-R M.2412-0: Guidelines for evaluation of radio interface technologies for IMT-2020,” International Telecommunication Union, Tech. Rep., Oct. 2017.
- [2] G. Durisi, T. Koch, and P. Popovski, “Towards massive, ultra-reliable, and low-latency wireless communication with short packets,” *Proc. IEEE*, vol. 104, no. 9, pp. 1711–1726, Sep. 2016.
- [3] Y. Polyanskiy, H. V. Poor, and S. Verdú, “Channel coding rate in the finite blocklength regime,” *IEEE Trans. Inf. Theory*, vol. 56, no. 5, pp. 2307–2359, May 2010.
- [4] W. Yang, G. Durisi, T. Koch, and Y. Polyanskiy, “Quasi-static multiple-antenna fading channels at finite blocklength,” *IEEE Trans. Inf. Theory*, vol. 60, no. 7, pp. 4232–4265, Jul. 2014.
- [5] G. Durisi, T. Koch, J. Östman, Y. Polyanskiy, and W. Yang, “Short-packet communications over multiple-antenna Rayleigh-fading channels,” *IEEE Trans. Commun.*, vol. 64, no. 2, pp. 618–629, Feb. 2016.
- [6] W. Yang, G. Caire, G. Durisi, and Y. Polyanskiy, “Optimum power control at finite blocklength,” *IEEE Trans. Inf. Theory*, vol. 61, no. 9, pp. 4598–4615, Sep. 2015.
- [7] J. Östman, G. Durisi, E. G. Ström, M. C. Coşkun, and G. Liva, “Short packets over block-memoryless fading channels: Pilot-assisted or noncoherent transmission?” Dec. 2017. [Online]. Available: <https://arxiv.org/abs/1712.06387>
- [8] S. Alamouti, “A simple transmit diversity technique for wireless communications,” *IEEE J. Sel. Areas Commun.*, vol. 16, no. 8, pp. 1451–1458, Oct. 1998.
- [9] J. L. Jensen, *Saddlepoint Approximations*. Oxford, U.K.: Oxford Univ. Press, 1995.
- [10] J. Scarlett, A. Martinez, and A. Guillén i Fàbregas, “Mismatched decoding: Error exponents, second-order rates and saddlepoint approximations,” *IEEE Trans. Inf. Theory*, vol. 60, no. 5, pp. 2647–2666, May 2014.
- [11] 3GPP, “TS 36.104: Technical specification group radio access network,” 3GPP, Tech. Rep., 2012.
- [12] —, “TR 38.901: Study on channel model for frequencies from 0.5 to 100 GHz,” 3GPP, Tech. Rep., 2017.
- [13] N. Merhav, G. Kaplan, A. Lapidoth, and S. Shamai (Shitz), “On information rates for mismatched decoders,” *IEEE Trans. Inf. Theory*, vol. 40, no. 6, pp. 1953–1967, Nov. 1994.
- [14] A. Martinez and A. Guillén i Fàbregas, “Saddlepoint approximation of random-coding bounds,” in *Proc. Inf. Theory Applicat. Workshop (ITA)*, San Diego, CA, U.S.A., Feb. 2011.
- [15] G. Kaplan and S. Shamai (Shitz), “Information rates and error exponents of compound channels with application to antipodal signaling in fading environment,” *Int. J. Electron. Commun. (AEÜ)*, vol. 47, no. 4, pp. 228–239, Jul. 1993.
- [16] 3GPP, “TR 38.913: Study on scenarios and requirements for next generation access technologies,” 3GPP, Tech. Rep., 2017.
- [17] Ericsson, “R1-1720997: On PDCCH for ultra-reliable transmission,” 3GPP, Tech. Rep., 2017.